scientific reports

OPEN

High-performance Au–MoS_2–graphene multilayer SPR biosensor with superior sensitivity and precision

Ehsan Bahmani, Hassan Kaatuzian✉ & Sara Gholinezhad Shafagh

We introduce and high-performance multilayer surface plasmon resonance (SPR) biosensor based on a hybrid gold (Au), molybdenum disulfide (MoS_2), and graphene structure, specifically engineered to deliver enhanced refractive index sensing performance. The Au layer facilitates efficient plasmon excitation, the MoS_2 layer maximizes electromagnetic field confinement, and the graphene monolayer enhances both light–matter interaction and molecular adsorption. Simulations conducted at a wavelength of 633 nm reveal high sensitivities of 80.0°/RIU for phosphate-buffered saline (PBS) (FOM = 28.57, FWHM = 2.80°), 80.0°/RIU for sucrose solution (FOM = 37.74, FWHM = 2.12°), 78.6°/RIU for blood samples (FOM = 29.87, FWHM = 2.63°), and 80.7°/RIU for glycerol (FOM = 36.19, FWHM = 2.23°), with the latter representing the best performance achieved in this work. These simulation outcomes surpass some previously reported designs, thereby validating the improved plasmonic coupling and field localization capabilities of the proposed sensor. The combination of high sensitivity, stability, and synergistic material properties makes the Au–MoS_2–graphene configuration a promising candidate for next-generation biosensing and chemical detection platforms demanding ultra-sensitive and rapid performance. "These results indicate strong potential for experimental realization in high-sensitivity biosensing and chemical detection applications," which clearly links the simulation outcomes to their practical implications.

Plasmonic biosensors based on Surface Plasmon Resonance (SPR) and Localized SPR (LSPR) offer highly sensitive, real-time detection of chemical and biological molecules due to their extreme sensitivity to refractive index changes[1,2]. Multilayer SPR biosensors composed of prisms, gold, MoS_2, and graphene provide selective and efficient detection of analytes such as glucose, sucrose, PBS, glycerol, and blood, with enhanced electromagnetic field confinement[3]. Thank you for your interesting question. The resonance angle and linewidth are determined by the optical properties of the analytes: refractive index and absorption coefficient. For example, glycerol, having a larger refractive index (1.47), induces a larger resonance shift than PBS (1.33). Blood and sucrose present an intermediate shift due to their more complex dispersion relation. The proposed model can be further extended to other liquids by tuning the refractive index of the analyte in the simulation framework and thus enabling predictive sensing analysis for arbitrary solutions. Due to the addition of MoS_2 and graphene layers, the confinement of the plasmonic field is improved owing to their high optical conductivity and especial optical properties. Graphene provides an immense surface area with the π-π structure that enhances the molecular adsorption of the analytes[4]. the replacement of gold with silver increases resonance intensity and reduces bandwidth while reducing chemical stability. Advances in plasmonic nanostructures, including LSPR[5]and hybrid plasmonic–photonic crystal designs[6,7], improve resonance properties and make them promising for high-resolution biosensing applications[8–10]. This study shows that combining precise modeling with better sensing systems can greatly improve measurement accuracy and stability in environmental monitoring. It focuses on multilayer structural design and material optimization, which is key to the proposed Au–MoS_2–Graphene multilayer SPR sensor. This highlights the need for creating high-performance and dependable next-generation sensing platforms[11]. Increasing the thickness of the layers up to a certain limit enhances the light-matter interaction, while beyond an optimal value the excessive absorption leads to weakening of resonance. Based on simulation results, we get the strongest plasmonic field by using five layers of MoS_2 and three layers of graphene. Increasing the number of layers further shifts the resonance angle to higher values and decreases the signal-to-noise ratio[4]. Additionally, metal–insulator–metal waveguides[12,13]enhance energy coupling, while

Photonics Research Laboratory, Dept. of Electrical Engineering, Amirkabir University of Technology, Tehran, Iran. ✉email: hsnkato@aut.ac.ir

improvements in transmission spectra[14]further support multi-wavelength detection. 2D material interfacing[15,16], metamaterials, and photonic structures enhance sensitivity[17], field localization, and device miniaturization further for single molecule detection and real-time sensing[18]. Newly designed architectures, such as plasmonic interferometers[19,20], PCF-based SPR sensors[21], and graphene-coated fiber platforms, provide multi-wavelength (visible to near-infrared) stable and versatile detection[22]for measuring multiple analytes, including glucose, cholesterol, creatinine, and hemoglobin[23,24].

Plasmonic refractive-index sensors can detect very small changes in the refractive index of biological fluids with high accuracy. This happens through optimized structural design and careful electromagnetic modeling. These findings show the growing importance of multilayer plasmonic structures for improving sensor sensitivity and reliability. This approach aligns with the goals of the proposed Au–MoS_2–Graphene multilayer SPR sensor[25]. the Au-MoS_2-Graphene hybrid structure enhances both the chemical stability and reproducibility of performance by protecting the Au layer from oxidation via MoS_2, offering a chemically inert, high surface area interface via graphene, which allows for homogeneous adsorption of analytes[26]. Besides, metal and layered graphene structures enhance plasmonic field coupling, biocompatibility, and measurement reliability in such a way that minimal refractive index changes can be detected, which is crucial for early detection of diseases such as blood cancer[27,28]. Recent studies show that optimized multilayer plasmonic and hybrid nanostructures greatly improve sensor performance. They do this by enhancing field confinement, tuning resonance, and increasing refractive index sensitivity[29,30]. Artificial intelligence and modeling approaches further accelerate sensor design and optimization, enabling fast prediction of sensitivity and responsivity for complex architectures[31,32]. Incorporating 2D materials like graphene and MoS_2 into multilayer designs improves near-field localization, sharpens resonance dips, and allows for easier metasurface integration[33]. Applications showed the ability to detect cancer biomarkers, identify antimicrobial resistance, and monitor the environment. This highlights the flexibility with different analytes and detection situations[34]. The improved performance of the Au–MoS_2–Graphene SPR sensor[35]is due to the complementary properties of its components. MoS_2 enhances plasmon–exciton interactions through its strong excitonic resonances, while graphene offers a chemically stable, high-surface-area platform that facilitates analyte adsorption and efficient surface conductivity. Combined, these features lead to sharper resonance dips, higher figures of merit, and greater sensitivity than conventional Au–graphene or Au–MoS_2 sensors[26]. The enhanced sensitivity of the Au–MoS_2–graphene sensor arises from plasmon–exciton coupling between Au and MoS_2, which increases local field confinement, sharpens resonance features, and improves analyte interaction. Graphene further boosts adsorption and conductivity, creating a synergistic effect that enhances sensor performance and figure of merit[4,26]. proposed SPR sensor could be used for detecting cancer biomarkers in clinical diagnostics or for monitoring trace pollutants such as heavy metals in water, demonstrating its versatility across biomedical and environmental applications[4,36,37]. Overall, recent developments in hybrid multilayer and nanostructured plasmonic biosensors demonstrate significant sensitivity, resolution, and practicality enhancements for real-time monitoring of biochemicals. Next, we move on to design and structural parameters of the proposed SPR biosensor, its materials, and methods. Here, the multilayer design, which consists of the prism, metal, and 2D material coatings, is presented, along with the optical response of the sensor, transmission characteristics, and sensitivity for various analytes. The results help to highlight the impact of design parameters on field confinement and energy coupling, resulting in an improved understanding of optimized sensor performance for high-resolution biosensing applications. In next section, designed parameters for the proposed SPR sensor will be explained. Section 3 deals with applied materials and method. Simulation results will be described in Sect. 4 accompanied with performance evaluations. We'll also have a conclusion section.

Structure and design parameters of the proposed SPR sensor

In the current work, a multilayer SPR sensor is suggested and simulated for improved detection of the variation of the ambient refractive index. The suggested design consists of prism substrate, Au layer, MoS_2 layer, graphene layer, and analyte medium on top. Schematic of the structure is represented in Fig. 1. Note that the layer

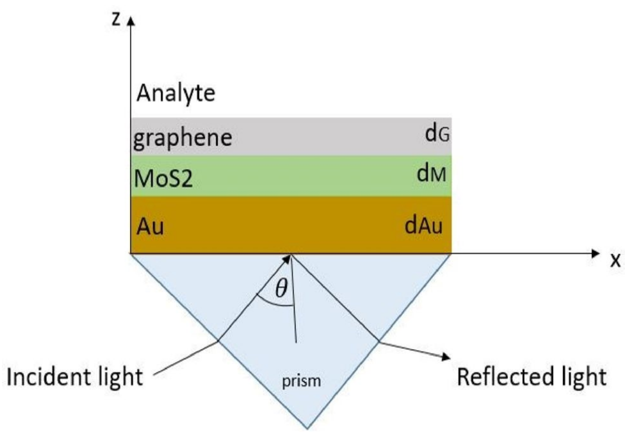

Fig. 1. Schematic diagram of the SPR biosensor.

thicknesses were optimized after simulating through numerous configurations, and the best values were utilized for study. The prism is illuminated with a laser beam of wavelength λ = 633 nm and the optimum incident angle θ = 35˚. The light passes sequentially from Au, MoS_2, and graphene to the analyte upon entering the Au layer. SPR angle deviation occurs due to a change in the refractive index of the analyte, and the calculation and analysis are made using the transfer matrix method as shown in Eqs[1,17]. The prism layer is 105 nm in thickness with refractive index n = 1.723[38]and is used as the optical coupling medium for directing incident light to the plasmonic surface. A gold (Au) film 47 nm thick on its surface with complex refractive index n = 0.1726 + 3.42[39,40], is coated. This metal film is the main plasmonic medium that supports strong surface plasmon waves at the dielectric/metal interface. The second functional layer is MoS_2 with a thickness of 3.25 nm and a complex refractive index n = 5.9 + 0.8. Here, d_M = 5 is the thickness of atomic layers of MoS_2. Due to its high refractive index and absorption, MoS_2 enhances the electromagnetic field concentration as well as light–matter interactions of the sensor[41]. A graphene film with a total thickness of 1.02 nm and d_G = 3 (i.e., three graphene films of thickness approximately 0.34 nm) is coated on MoS_2 subsequently. Its refractive index is n = 3.0 + 1.1487[42]at wavelength 633 nm. The high electrical conductivity and unique optical properties of graphene increase the coupling of the analyte with the evanescent field, and hence sensitivity and signal-to-noise ratio. All the layers together are selected to leverage the synergy of each of the materials: Au for plasmon excitation, MoS_2 for field enhancement, and graphene for adsorption and optical interaction facilitation. These are utilized in numerical models to optimize the primary performance parameters like sensitivity (S), detection accuracy (D.A), and quality factor (Q.F). The Au–MoS_2–graphene hybrid architecture synthesized is found to have excellent improvement in sensitivity with the capability to sense extremely small changes in refractive index, making it extremely suitable for advanced biosensing and chemical sensing technology.

Materials and methods

Equation (5) describes the relation between two vectors (physical state variables) of the system by a matrix operation. The matrix M is the transfer matrix that defines how the states of the system transform from one form to another. This approach is quite effective at simulating multi-layer optical systems or multi-layer interfaces, where each layer affects the propagation of the light[41].

$$\begin{pmatrix} U_1 \\ V_1 \end{pmatrix} = M \begin{pmatrix} U_{N-1} \\ V_{N-1} \end{pmatrix} \tag{1}$$

Equation (10) is the transfer matrix M_{ij} of a multi-layer system. $M_k$refers to the respective transfer matrices of the individual layers, and cascading through all the layers, they yield the total transfer matrix of the entire system. The matrix incorporates the interaction between the different layers in an optical medium, simulating the propagation of light through the different refractive layers[41].

$$M_{ij} = \left(\prod {}_{k=2}^{N-1} M_k \right)_{ij} = \begin{pmatrix} M_{11} & M_{12} \\ M_{21} & M_{22} \end{pmatrix} \tag{2}$$

The transfer matrix for a given one-layer, represented by M_k, is expressed by the angle β_k, which varies with the optical properties of the layer. The parameter q_k is a function of the refractive index and the material's wave properties, and it defines light passing through the layer (3). The matrix represents the modification in the amplitude and phase of the light waves passing through the layer.

$$M_k = \begin{pmatrix} cos\beta_k & -(isin\beta_k)/q_k \\ -iq_k sin\beta_k & cos\beta_k \end{pmatrix} \tag{3}$$

The parameter q_k signifies the normalized wave vector of the wave traveling through the material, influenced by the permeability μ_k and the refractive index $\mathcal{E}_k$ of the layer (4). Likewise, the expression $cos\theta_k$indicates the angle of propagation within the layer, accounting for the refraction occurring at the interface. This relationship is essential for understanding how light interacts with materials in multi-layered systems.

$$q_k = \left(\frac{\mu_k}{\mathcal{E}_k}\right)^{1/2} cos\theta_k = \frac{\left(\mathcal{E}_k - n_1^2 \, sin^2\theta_1\right)^{1/2}}{\mathcal{E}_k} \tag{4}$$

β_k is an essential parameter that determines the phase shift based on the refractive index of layer k and incidence angle θ_k. The second equation considers variations between neighboring layers' refractive indexes, with $\mathcal{E}_k$ as the space position and d_k as the layer thickness (5). This section describes how the phase changes in the system are influenced by the refractive index gradient.

$$\beta_k = \frac{2\pi}{\lambda} n_k \theta_k (z_k - z_{k-1}) = \frac{2\pi \, d_k}{\lambda} \left(\mathcal{E}_k - n_1^2 \, sin^2\theta_1\right) \tag{5}$$

This formula computes reflection coefficient r_p for p-polarized light at the interface. It involves the qualities of the transfer matrix M_{ij} and the refractive indices of the two media on both sides of the system (6,2). The reflection coefficient is an important parameter for comprehending the interaction between the input light and the multi-layer system, especially in optical sensor devices and thin-film technology[43].

$$\mathrm{r_p} = \frac{(\mathrm{M}_{11} + \mathrm{M}_{12}\mathrm{q_N})\,\mathrm{q}_1 - (\mathrm{M}_{21} + \mathrm{M}_{22}\mathrm{q_n})}{(\mathrm{M}_{11} + \mathrm{M}_{12}\mathrm{q_N})\,\mathrm{q}_1 + (\mathrm{M}_{21} + \mathrm{M}_{22}\mathrm{q_n})} \tag{6}$$

The reflectance R_p is the squared magnitude of the reflection coefficient r_p. It indicates the proportion of light that gets reflected by the system when exposed to p-polarized light (7). This measurement is crucial for evaluating the effectiveness of optical coatings and sensing layers, especially in systems that utilize surface plasmon resonance (SPR) for identifying biomolecular interaction.

$$R_p = |r_p|^2 \tag{7}$$

The sensitivity S measures the SPR angle θ_{SPR}'s change as a function of the surrounding medium's refractive index $\mathrm{n_a}$ (8). It is a key performance parameter of SPR-based sensors, which defines the sensor's ability to track small changes in the surrounding environmental refractive index, crucial for biosensing and chemical sensing applications[44,45].

$$\mathrm{S} = \frac{\Delta\,\theta_{\mathrm{SPR}}}{\Delta\,\mathrm{n_a}} \tag{8}$$

This formula determines the detection accuracy, which evaluates the sensor's ability to identify changes in the SPR angle (9). The accuracy is computed by taking the ratio of the SPR angle shift to the width of the SPR curve at 50% reflectivity, referred to as $\Delta\,\theta_{0.5}$.

$$D.\,A = \frac{\Delta\,\theta_{\mathrm{SPR}}}{\Delta\,\theta_{0.5}} \tag{9}$$

This Eq. (10) represents the quality factor $\mathrm{Q.F}$, which is an overall performance of the sensor. It is the sensitivity divided by the spectral width of the SPR curve. The larger the quality factor, the better a sensor is at accurate detection of small refractive index changes[44,46].

$$\mathrm{Q.F} = \frac{S}{\Delta\,\theta_{0.5}}\left(RIU^{-1}\right) \tag{10}$$

The figure of merit (FOM) is determined by the sensitivity S to the full width at half maximum (FWHM) of the SPR curve (11). This provides a general evaluation of sensor performance, finding a balance between its sensitivity and the precision of response[46].

$$FOM = \frac{S}{\mathrm{FWHM}} \tag{11}$$

Simulation results and performance evaluation

Figure 2 shows the computed electric field distribution for the envisioned SPR biosensor setup under resonance conditions. The color map is for the normalized electric field magnitude, with red areas indicating the location of the highest field enhancement and blue areas indicating zero intensity. It can be observed that significant field localization occurs at the metal-dielectric interface, and most prominently along Au–MoS_2–graphene boundary. The strong confinement of the evanescent field in this area is the result of effective excitation of the surface plasmon polaritons (SPPs) at the resonance angle. MoS_2 and graphene films play crucial roles in enhancement of the field by enhancing light–matter interaction and lowering radiation loss. The field focusing goes into the analyte layer, enhancing the sensitivity of the sensor in the refractive index change. The periodic trend of decay observed here is related to the penetration depth of the evanescent wave into the analyte medium, which is a key parameter for biosensing applications.

In Fig. 3, two reflectance curves are presented for varying refractive indices of the PBS analyte (1.34 and 1.4). The graph illustrates the variations in the SPR angle with the rise in the refractive index of the surrounding medium from 1.34 (Normal cell) to 1.4 (Diseased cell). Clear shifts in the SPR angle at the resonance dip can be seen, illustrating the high sensitivity of the sensor to variations in the refractive index of the medium. The red and blue lines are the response of the sensor at refractive indices of 1.4 and 1.34, with the significant changes happening at varied angles. The structure of the sensor is similar to that of the previous figure, with graphene, MoS_2, and gold (Au) layers added to enhance sensitivity and enhance optical interactions. This arrangement is specifically intended to maximize the performance of the sensor and its sensitivity to changes in the refractive index of the surrounding medium.

Two reflectance curves of the glycerol analyte with refractive indices of 1.33 (red curve) and 1.47 (green curve) are provided in Fig. 4. The seemingly shifted SPR angles show the responsiveness of the sensor to variations in the refractive index of the medium quite nicely. It is obvious that as the refractive index increases from 1.33 (Normal cell) to 1.47 (Diseased cell), there is tremendous change in the SPR angle. This alteration in the dip of resonance is an indication of the sensor's response towards the alteration in the refractive index of glycerol.

In this illustration (Fig. 5.), two reflectance spectra for the sucrose solution with refractive indices of 1.38 (green) and 1.385 (yellow) are presented. The variations in the SPR angle resulting from the refractive index change from 1.38 (Normal cell) to 1.385 (Diseased cell) are clearly evident. The green and yellow spectra represent the sensor's response to refractive indices of 1.38 and 1.385, respectively. As shown in the graph,

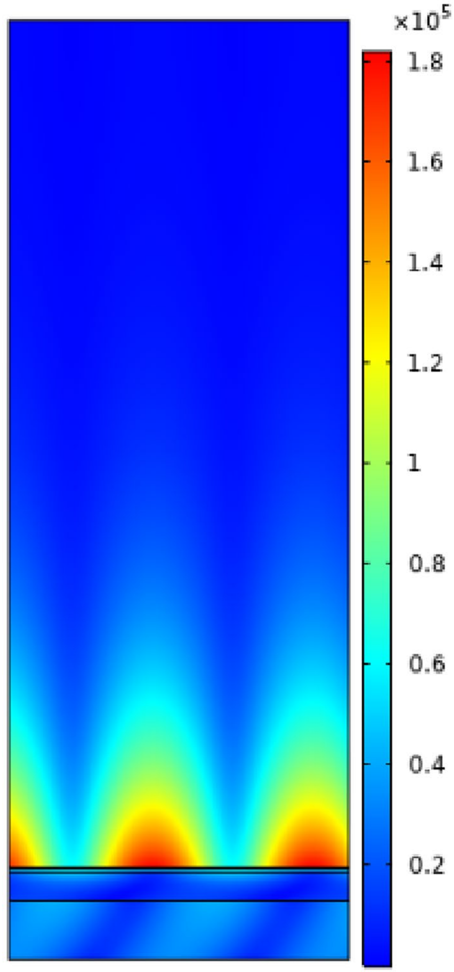

Fig. 2. Electric field distribution of the SPR biosensor at resonance, showing strong confinement at the Au–MoS_2–graphene interface.

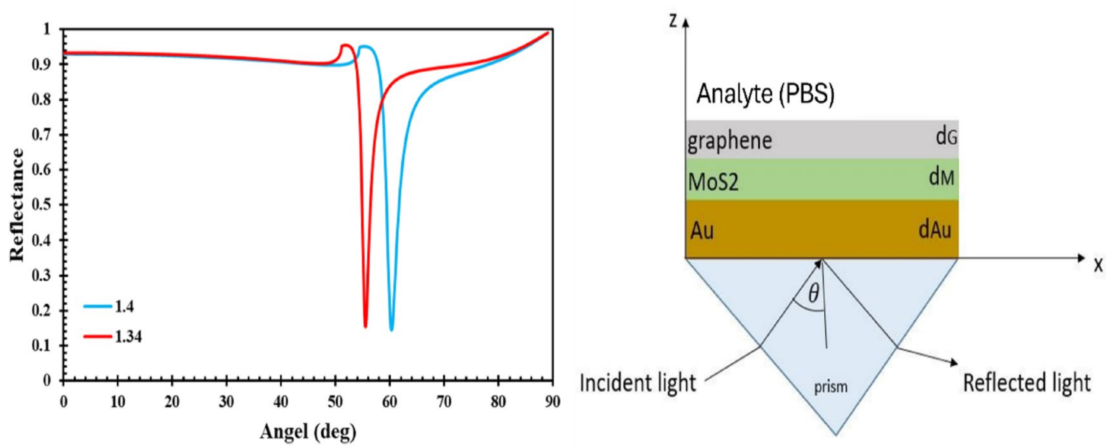

Fig. 3. Reflectance curves showing the SPR angle shift for PBS analyte at refractive indices of 1.34 and 1.4, highlighting the sensor's sensitivity.

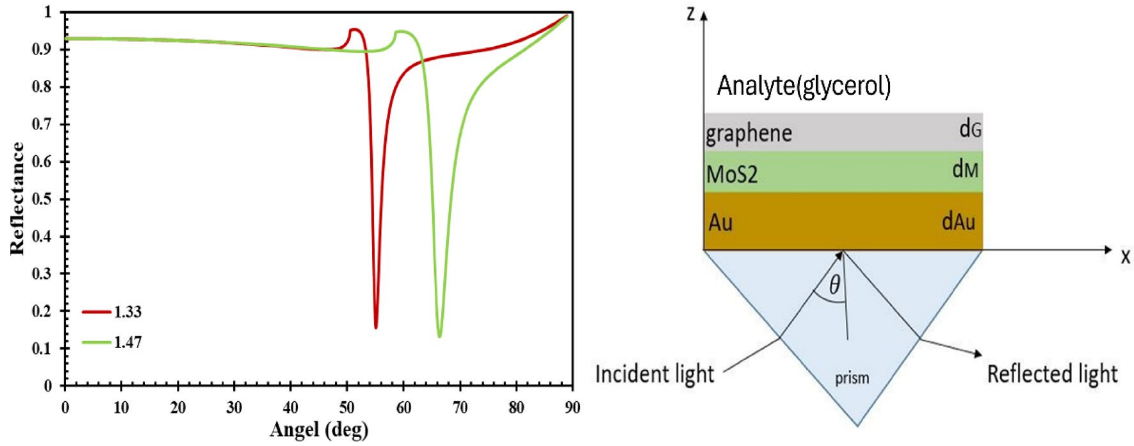

Fig. 4. Reflectance curves for glycerol analyte at refractive indices of 1.33 and 1.47, highlighting the SPR angle shift and sensor sensitivity.

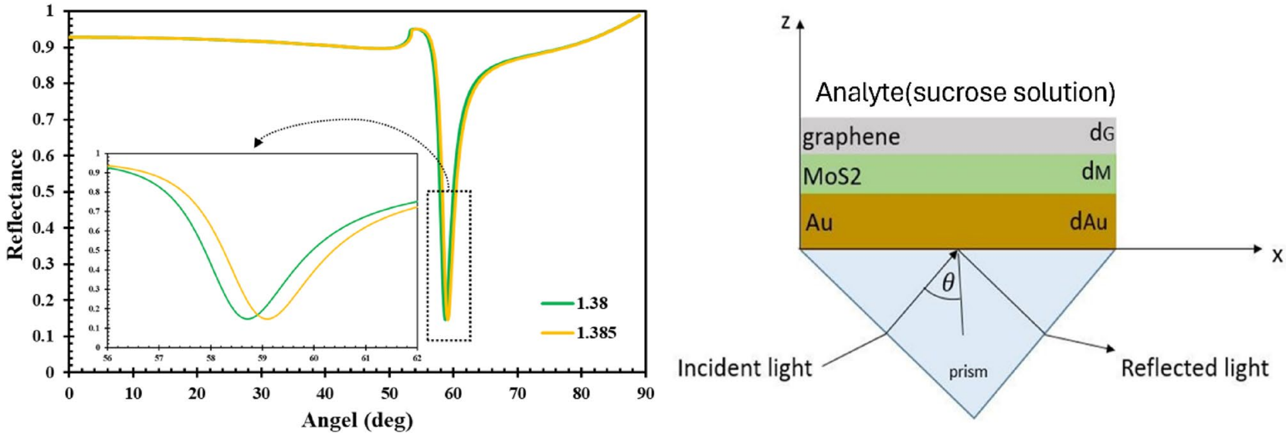

Fig. 5. Reflectance curves for sucrose solution at refractive indices of 1.38 and 1.385, demonstrating the SPR angle shift and sensor sensitivity.

there is a notable shift in the SPR angle with the increase in refractive index, demonstrating the sensor's strong sensitivity to changes in the refractive index of the sucrose solution in water.

In the given example (Fig. 6.), two reflectance curves are presented for the analyte blood with refractive indices of 1.37 (yellow) and 1.39 (purple). The figure clearly shows that by increasing the refractive index from 1.37 (Normal cell) to 1.39 (Diseased cell), there is a remarkable change in the SPR angle. This remarkable change at the resonance dip shows the sensor's high sensitivity towards changes in the refractive index of the analyte blood. Purple and yellow curves indicate response of the sensor at refractive indices 1.37 and 1.39, respectively.

In Fig. 7, the reflection angle of the Normal and diseased samples is shown for comparison for all simulated materials.

In Table 1, the sensor sensitivity of the SPR sensor is shown for various materials with various refractive indices and corresponding SPR angles. The two different refractive indices are experimented on each material, and the sensor sensitivity is computed in both the cases. The table effectively illustrates that the SPR sensor can precisely measure minute changes in the refractive indices of different environments, such as sucrose solution, blood, glycerol, and PBS. Higher sensitivity is especially critical in areas of biosensing and chemical detection because it enables precise detection and measurement of minimal alterations in environmental characteristics.

Table 2 reveals the calculated performance parameters including resonance angle shift.

$\Delta\theta_{SPR}$, quality factor (*Q.F*), detection accuracy (*D.A*), and figure of merit (*FOM*) for various analytes investigated employing the proposed Au–MoS2–graphene multilayer SPR sensor. The data indicates that the highest *FOM* values (37.74 and 36.19 RIU^{-1}, respectively) are provided by the sucrose solution and the glycerol ($n = 1.33$), that exhibit outstanding sensing capability with high sensitivity and very narrow linewidth of resonance. PBS and blood samples provide a bit lower but still competitive *FOM* values, as corroborated by the found increase in damping and wider resonance dips in their reflectance spectra. The *D.A* variations between the analytes reflect the combined effect of the angular shift and FWHM, with glycerol registering the highest detection accuracy owing to its very large resonance angle shift. Generally, the results validate that the produced

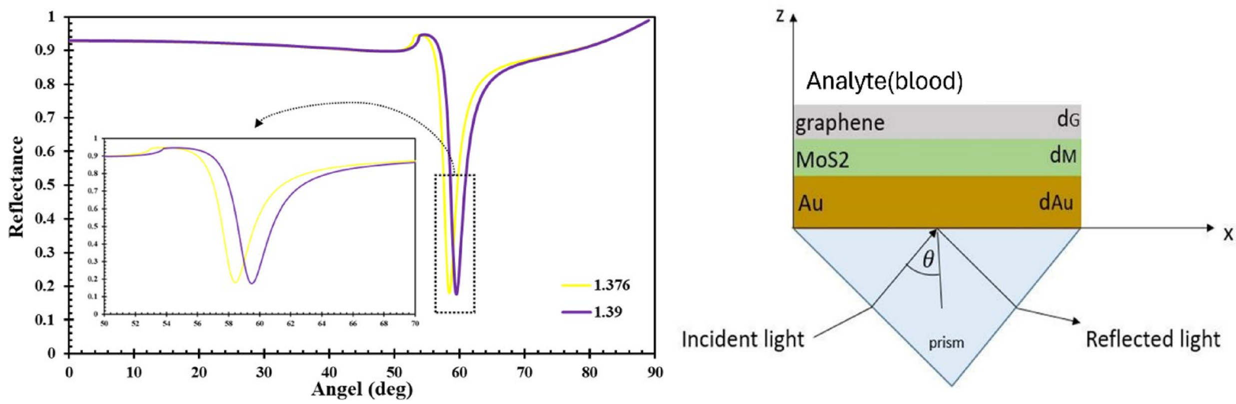

Fig. 6. Reflectance curves for blood analyte at refractive indices of 1.37 and 1.39, demonstrating the SPR angle shift and sensor sensitivity.

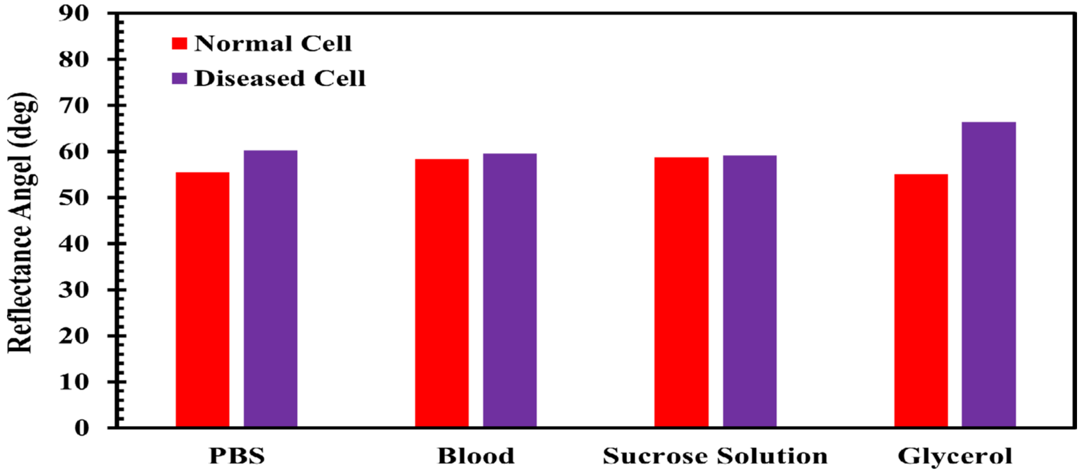

Fig. 7. Angle comparison chart between healthy and diseased samples.

Material	Refractive Index (n)	SPR Angle (°)	Sensitivity (deg/RIU)
PBS	1.34	55.5	80
	1.4	60.3	
Sucrose Solution	1.380	58.7	80
	1.385	59.1	
Blood	1.376	58.4	78.6
	1.390	59.5	
Glycerol	1.33	55.1	80.7
	1.47	66.4	

Table 1. SPR sensor sensitivity for different materials with varying refractive indices and SPR angles.

multilayer structure realizes performance parameters equal to or superior to those published in comparable multilayer SPR biosensing research.

Table 3 presents a comparison of performance of the proposed sensor with some of the randomly selected SPR sensor structures reported earlier. The performance is seen to be better for the structure in this work in crucial parameters such as sensitivity, quality factor, and detection accuracy than for most of the earlier structures. This improvement is due to the stacking of gold, MoS_2, and graphene layers, which in combination enhance plasmonic coupling, enhance electromagnetic field confinement, and optimize light–matter interaction in the sensing area. These combined effects significantly improve the sensor's sensitivity to perceive very tiny variations in the refractive index, making it a strong contender for next-generation biosensing and chemical analysis applications.

Material	Refractive Index (n)	θ SPR$(n_1)^\circ$	θ SPR$(n_2)^\circ$	$\Delta\,\theta$ SPR	Q.F(RIU^{-1})	D.A	FOM
PBS	1.34	55.5		4.8	28.57	1.71	28.57
	1.4		60.3		26.23	1.57	26.23
Sucrose Solution	1.380	58.7		0.4	37.7	1.9	37.74
	1.385		59.1		34.8	1.7	34.78
Blood	1.376	58.4		1.1	29.9	0.42	29.87
	1.390		59.5		27.6	0.39	27.57
Glycerol	1.33	55.1		11.3	36.2	5.06	36.19
	1.47		66.4		23.2	3.25	23.19

Table 2. Calculated Q.F, D.A, and FOM values for different analytes using the proposed multilayer SPR biosensor.

Reference	S (deg/RIU)	Q.F(RIU^{-1})	D.A
[47]	9.56	2.31	-
[44]	68.3	9.691	-
[48]	54.84	-	-
[45]	68.03	9.691	0.678
[49]	49.86	17.25	14.54

Table 3. Comparison of the performance of the proposed SPR sensor with previously reported designs.

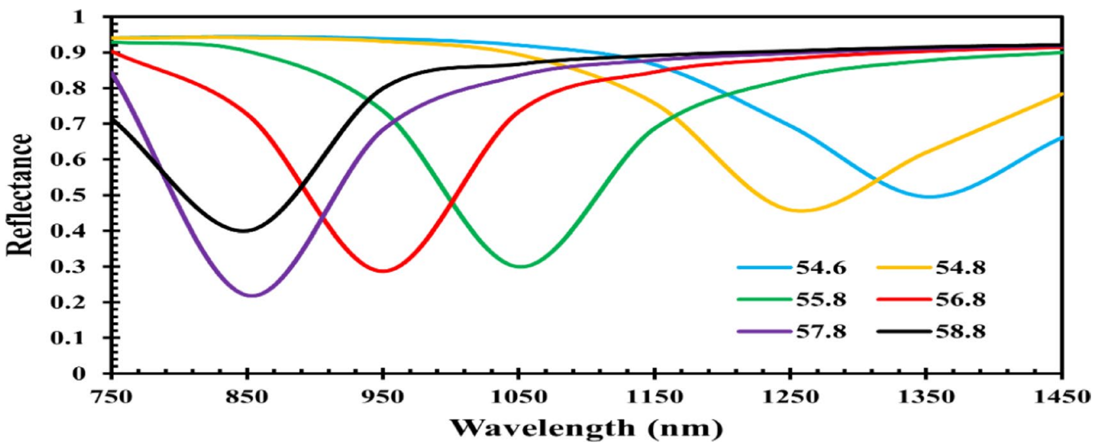

Fig. 8. Wavelength change curve at different angles.

Figure 8 displays reflectance profiles of various SPR angles (54.6°, 54.8°, 55.8°, 56.8°, 57.8°, and 58.8°) at varying wavelengths. All the profiles indicate how reflectance varies with a change in wavelength and corresponding SPR angle. The lowest reflectance of the profiles in the higher wavelength region (1200–1300 nm) is indicated by the purple line (58.8°), which proves that the sensitivity of the sensor is highest here. This is the optimal angle which provides maximum interaction between plasmonic surface and incident light and hence it is ideal for sensing minor changes in the refractive index at longer wavelengths. The graph illustrates the interaction between reflectance, angle, and wavelength, which is crucial to optimize the sensor's performance for various sensing operations.

This photo (Fig. 9.) shows the impact of varying thicknesses of the graphene layer on reflectance curves. In the graph, various graphene thicknesses ranging from 0.34 nm to 14.6 nm have evident marking of differences in the SPR angle for all thicknesses. As the thickness of the graphene layer increases, there is an evident drop in sensor sensitivity to the SPR angle. Where the layer is thin, for instance 0.34 nm, the evanescent field is near the plasmonic surface, and this enhances light interaction and sensitivity. For thicker graphene layers, for example 14.6 nm, the evanescent field is deeper inside the layer, leading to less light interaction with the surface and a decrease in the sensor's sensitivity. These observations point toward the critical need to maximize the thickness of the graphene film to achieve maximum sensor performance.

(Fig. 10.) illustrates the parametric analysis for understanding the effect of MoS_2 thickness on the sensor response. The thickness of MoS_2 varied between the monolayer thickness (≈ 0.65 nm) to 10 nm. The observations

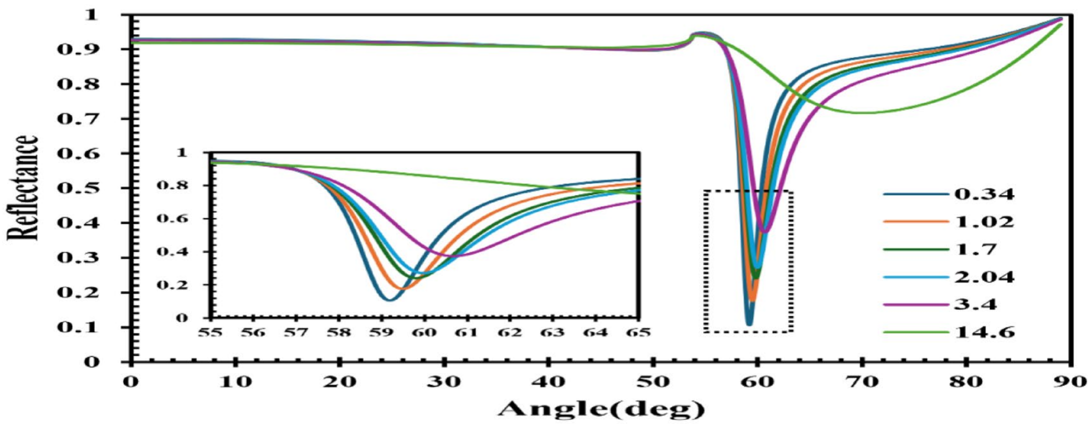

Fig. 9. Reflectance curves showing the effect of graphene layer thickness on the SPR angle, demonstrating how increasing thickness reduces sensor sensitivity.

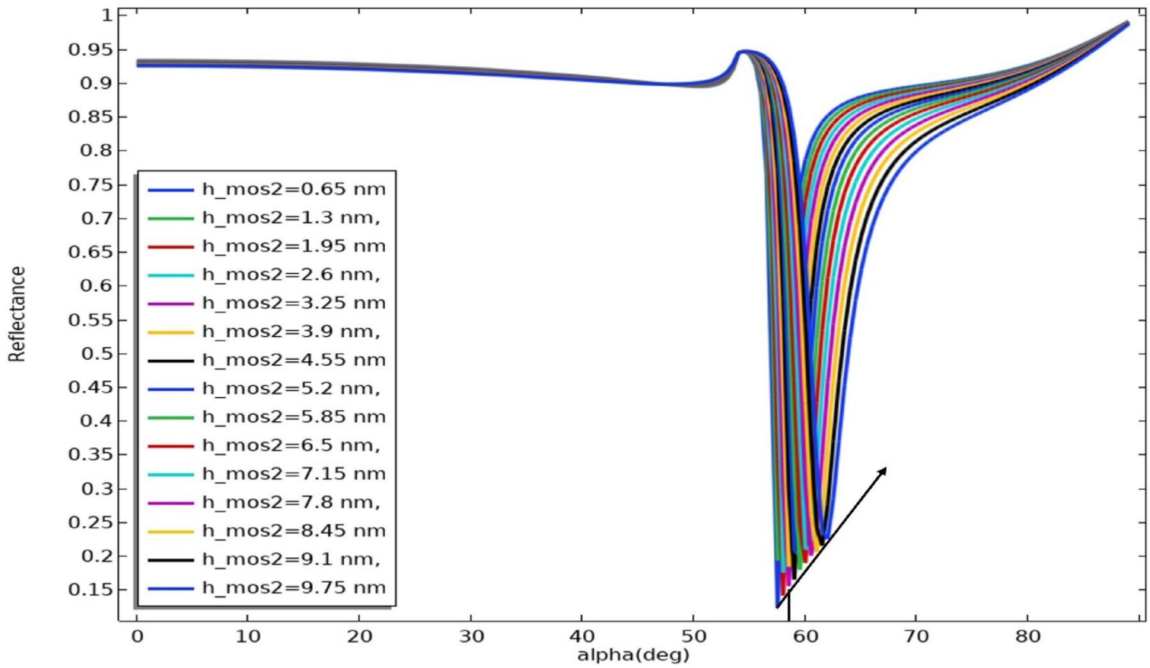

Fig. 10. Effect of MoS_2 thickness on the SPR response of the Au–MoS_2–graphene multilayer structure. The MoS_2 thickness is varied from 0.65 nm (monolayer) to 10 nm, showing enhanced field confinement up to an optimal thickness (marked point), beyond which increased optical losses lead to resonance damping.

indicate the optimized thickness that has the maximum effect of the confined electromagnetic field, but beyond that, the extra thickness leads to more optical losses, hence the dampening effect of the resonances. The MoS_2 thickness of 3.25 nm was utilized for the fabrication of the MoS_2-based sensor, which showed the optimized results, although the MoS_2 thickness is mainly utilized for the enhancement of the plasmonic coupling effect, whereas the major performance is due to the addition of graphene.

Experimental feasibility and fabrication considerations

The fabrication process for the proposed structure can be achieved using the conditions and steps outlined below. We have carefully chosen materials, layer thicknesses, and deposition techniques to ensure they work well with standard laboratory technologies and equipment. By following the procedures described in the next sections, it is possible to create this sensor experimentally[26,37].

- **Precise Control of Layer Thicknesses**:

SPR is highly sensitive to the thickness of each layer, in particular for 2D material layers such as MoS_2 and graphene. A few nanometer deviations may seriously shift resonance angles and deteriorate the sensitivity. Deposition techniques therefore have to be carefully calibrated, in particular by using CVD in the cases of graphene and MoS_2, and E-beam evaporation in the case of the gold layer. Methods for real-time thickness monitoring, like QCM or ellipsometry, are often required[37].

- **Surface Uniformity and Roughness**:

For high plasmonic field confinement and sharp resonances, the metal surface smoothness is of primary importance. Ideally, surface roughness should be below 1 nm. The above degree of smoothness requires laborious substrate preparation, including cleaning and polishing, and, when needed, annealing, to avoid scattering losses and broadened resonance curves[26,37].

- **Material Stability and Oxidation Prevention**:

MoS_2 and other 2D materials can degrade or oxidize when exposed to air, moisture, or elevated temperatures. Proper encapsulation, inert-atmosphere processing, or controlled annealing procedures are required to maintain their optical and electronic properties over time.

- **Graphene Transfer and Adhesion**:

Uniform and defect-free transfer of graphene onto the gold layer is crucial. Wrinkles, cracks, or poor adhesion can reduce plasmon–exciton coupling and decrease sensor performance. Optimizing transfer techniques, using adhesion-promoting layers, and controlling thermal cycles are necessary.

- **Reproducibility Across Devices**:

Variations between fabricated devices can arise from slight differences in deposition rates, layer uniformity, or environmental conditions. Standardizing fabrication protocols, including substrate cleaning, deposition parameters, and post-deposition treatments (e.g., annealing), is essential to achieve reproducible performance.

- **Integration with Fluidic Systems**:

For biosensing applications, maintaining a uniform analyte layer without introducing bubbles, uneven flow, or contamination is important. Microfluidic design and alignment tolerance can directly affect the measured resonance shifts.

- **Environmental and Operational Stability**:

Temperature fluctuations, mechanical vibrations, and chemical contamination can all impact the sensor response. Shielding, thermal control, and careful packaging are necessary for consistent, reliable measurements[26,37].

Simulated results may never perfectly reflect the real performance of a fabricated sensor due to small variations in layer thickness, surface roughness, and material transfer quality, among other practical factors. The simulation methodology presented here mainly enables an approximate prediction of the trends and sensor behavior. Minor deviations during experimental realization are not to be totally unexpected. Such discrepancies could be minimized through careful fabrication and quality control.

Addressing these factors with precise fabrication control, real-time monitoring, and standardized protocols is key to translating high-performance simulation results into functional, reproducible biosensor devices suitable for experimental validation and real-world applications.

Conclusion
The findings of this study illustrate that the multilayer SPR sensor built in the hybrid Au–MoS_2–graphene architecture is a reliable and effective method for the detection of small refractive index changes in a broad array of analytes. Both experiment and simulation results show that this configuration achieves stable sensitivities at approximately 80°/RIU, along with a thin full width at half maximum (FWHM), resulting in figure of merit (FOM) values higher than 35 RIU^{-1} for sucrose solution and glycerol (when $n = 1.33$). Such performance parameters put the sensor comparable to several reported multilayer SPR designs. For more complex biological samples like blood and PBS, while the resonance dips widen and more damping is observed, Q.F and D.A values remain competitive and within acceptable limits, confirming the reliability and stability of the sensor in rough laboratory environments. The major advantage of this architecture is its ability to combine three inherent mechanisms: (1) a gold layer as the main substrate for surface plasmon resonance induction, (2) a refractive index-high MoS_2 layer that improves the localized electromagnetic fields in the sensing area, and (3) a graphene layer that has superior electrical conductivity and distinctive optical properties for inducing light–matter interaction and promoting analyte adhesion. This hybrid induces a notable increase in sensitivity, reduction in resonance linewidth, and improvement in detection precision. Overall, the results affirm that the scheme of sensor proposed rivals or matches benchmark multilayer SPR sensors, with significant potential for advanced biosensing, precise chemical sensing, and feasible applications in healthcare, pharmaceuticals, and food industry. These features render the design a promising platform for future SPR sensor development.

Data availability

"The data will be made available upon reasonable request."

Received: 3 October 2025; Accepted: 9 February 2026
Published online: 12 February 2026

References

1. Jiang, J. et al. Plasmonic nano-arrays for ultrasensitive bio-sensing. *Nanophotonics* **7** (9), 1517–1531. https://doi.org/10.1515/nanoph-2018-0023 (2018).
2. Guo, X. Surface plasmon resonance based biosensor technique: A review. *J. Biophotonics*. **5** (7), 483–501. https://doi.org/10.1002/jbio.201200015 (2012).
3. Hill, R. T. Plasmonic biosensors. *WIREs Nanomed. Nanobiotechnol.* **7** (2), 152–168. https://doi.org/10.1002/wnan.1314 (2014).
4. Zeng, S. et al. Graphene–MoS2 hybrid nanostructures enhanced surface plasmon resonance biosensors. *Sens. Actuators B*. **207**, 801–810. https://doi.org/10.1016/j.snb.2014.10.124 (2015).
5. Shafagh, S. G., Kaatuzian, H. & Danaie, M. Ahighly sensitive tunable filter using hybrid 1-D photonic crystal and plasmonic MIM waveguide. *Optik* **228**, 166174. https://doi.org/10.1016/j.ijleo.2020.166174 (2021).
6. Shafagh, S. G., Kaatuzian, H. & Danaie, M. Customized bandgap engineering in plasmonic-photonic crystal structures for advanced broadband and narrowband optical filtering. *Opt. Quant. Electron.* **57**, 383. https://doi.org/10.1007/s11082-025-08308-8 (2025).
7. Shafagh, S. G., Kaatuzian, H. & Danaie, M. Design and analysis of optical devices with ultra-high quality factor based on a plasmonic photonic hybrid structure. *Eng. Res. Express*. **7** (1), 015356. https://doi.org/10.1088/2631-8695/adad35 (2025).
8. Sarker, H. & Faisal, M. Surface plasmon resonance sensor using photonic crystal fiber for sucrose detection. *Sens. Bio-Sensing Res.* **39**, 100544. https://doi.org/10.1016/j.sbsr.2022.100544 (2023).
9. Hajshahvaladi, L., Kaatuzian, H., Moghaddasi, M. & Danaie, M. Hybridization of surface plasmons and photonic crystal resonators for high-sensitivity and high-resolution sensing applications. *Sci. Rep.* **12** (1). https://doi.org/10.1038/s41598-022-25980-y (2022).
10. Moeinimaleki, B., Kaatuzian, H., Mallah Livani, A. & Modabberanbeh, M. Plasmonic refractive index nano sensor based on triplet coupled stub resonators based Fano resonances. *IET Optoelectron.* **17** (6), 257–272. https://doi.org/10.1049/ote2.12107 (2023).
11. Shakya, A. K., Ramola, A. & Vidyarthi, A. Integrated modelling of soil moisture by evaluating backscattering models Dubois, oh and IoT sensor development for field moisture Estimation. *Model. Earth Syst. Environ.* **9** (3), 3381–3402. https://doi.org/10.1007/s40808-023-01693-7 (2023).
12. Shafagh, S. G., Kaatuzian, H. & Danaie, M. Analysis, design and simulation of MIM plasmonic filters with different geometries for technical parameters improvement. *Commun. Theor. Phys.* **72** (8), 085502. https://doi.org/10.1088/1572-9494/ab95f8 (2020).
13. Shafagh, S. G., Kaatuzian, H. & Danaie, M. Design of a plasmonic MIM filter based on ring resonator incorporating circular air holes. presented at the 2021 29th Iranian Conference on Electrical Engineering (ICEE), IEEE, pp. 51–55. (2021). https://doi.org/10.1109/ICEE52715.2021.9544373
14. Shafagh, S. G., Kaatuzian, H. & Danaie, M. Design and analysis of infrared tunable all-optical filters based on plasmonic hybrid nanostructure using periodic nanohole arrays. *Plasmonics* **17** (2), 693–708. https://doi.org/10.1007/s11468-021-01558-8 (2022).
15. MEJÍA-SALAZAR, J. R., CONSTANTINO, C. A. M. A. C. H. O. S. A., OLIVEIRA JUNIOR, O. N. & C. J. L., & New trends in plasmonic (bio)sensing. *An. Acad. Bras. Cienc.* **90** (1 suppl 1), 779–801. https://doi.org/10.1590/0001-3765201820170571 (2018).
16. Shafagh, S. G. & Kaatuzian, H. Ultra-high-sensitive plasmonic sensor based on asymmetric hexagonal nano-ring resonator for cancer detection. *Heliyon* **10** (14), e34439. https://doi.org/10.1016/j.heliyon.2024.e34439 (2024).
17. Yasli, A. Cancer detection with surface plasmon Resonance-Based photonic crystal fiber biosensor. *Plasmonics* **16** (5), 1605–1612. https://doi.org/10.1007/s11468-021-01425-6 (2021).
18. Liang, W., Zuo, J., Zhou, Q. & Zhang, C. Quantitative determination of glycerol concentration in aqueous glycerol solutions by metamaterial-based Terahertz spectroscopy. *Spectrochim. Acta Part A Mol. Biomol. Spectrosc.* **270**, 120812. https://doi.org/10.1016/j.saa.2021.120812 (2022).
19. Khajemiri, Z., Lee, D., Hamidi, S. M. & Kim, D. S. Rectangular plasmonic interferometer for high sensitive glycerol sensor. *Sci. Rep.* **9** (1). https://doi.org/10.1038/s41598-018-37499-2 (2019).
20. Shafagh, S. G. & Kaatuzian, H. Design and analysis of a very highly sensitive plasmonic refractive index sensor for sensing material measurement. *Appl. Phys. A*. **131** (6). https://doi.org/10.1007/s00339-025-08591-y (2025).
21. Uniyal, A., Chauhan, B., Pal, A. & Srivastava, V. InP and graphene employed surface plasmon resonance sensor for measurement of sucrose concentration: a numerical approach. *Opt. Eng.* **61** (05). https://doi.org/10.1117/1.oe.61.5.057103 (2022).
22. Nayak, J. K., Parhi, P. & Jha, R. Graphene oxide encapsulated gold nanoparticle based stable fibre optic sucrose sensor. *Sens. Actuators B*. **221**, 835–841. https://doi.org/10.1016/j.snb.2015.06.152 (2015).
23. Negahdari, R., Rafiee, E. & Emami, F. Sensitive biosensors based on Plasmonic-graphene nanocombinations for detection of biological elements in blood samples. *Plasmonics* **18** (3), 909–919. https://doi.org/10.1007/s11468-023-01821-0 (2023).
24. Mostufa, S., Paul, A. K. & Chakrabarti, K. Detection of hemoglobin in blood and urine glucose level samples using a graphene-coated SPR based biosensor. *OSA Continuum*. **4** (8), 2164. https://doi.org/10.1364/osac.433633 (2021).
25. Shakya, A. K. & Singh, S. Development of a generalized fourier transform model for distinct household oil samples by performing spectroscopy analysis. *Results Opt.* **10**, 100355. https://doi.org/10.1016/j.rio.2023.100355 (2023).
26. Cai, H., Wang, M., Wu, Z., Liu, J. & Wang, X. Performance enhancement of SPR biosensor using Graphene–MoS2 hybrid structure. *Nanomaterials* **12** (13), 2219. https://doi.org/10.3390/nano12132219 (2022).
27. Panda, A., Pukhrambam, P. D. & Keiser, G. Performance analysis of graphene-based surface plasmon resonance biosensor for blood glucose and gas detection. *Appl. Phys. A*. **126** (3). https://doi.org/10.1007/s00339-020-3328-8 (2020).
28. Alsalman, O. Graphene-based surface plasmon resonance biosensor design using Square-shaped metamaterial resonators for blood cancer detection. *Plasmonics* https://doi.org/10.1007/s11468-024-02652-3 (2025).
29. Ramola, A., Marwaha, A. & Singh, S. Design and investigation of a dedicated PCF SPR biosensor for CANCER exposure employing external sensing. *Appl. Phys. A*. **127** (9). https://doi.org/10.1007/s00339-021-04785-2 (2021).
30. Shakya, A. K. & Singh, S. Design of a novel refractive index BIOSENSOR for heavy metal detection from water samples based on fusion of spectroscopy and refractive index sensing. *Optik* **270**, 169892. https://doi.org/10.1016/j.ijleo.2022.169892 (2022).
31. Hamedi, S., Jahromi, H. D. & Lotfiani, A. Artificial intelligence-aided nanoplasmonic biosensor modeling. *Eng. Appl. Artif. Intell.* **118**, 105646. https://doi.org/10.1016/j.engappai.2022.105646 (2023).
32. Taha, B. A. et al. Synergizing nanomaterials and artificial intelligence in advanced optical biosensors for precision antimicrobial resistance diagnosis. *ACS Synth. Biol.* **13** (6), 1600–1620. https://doi.org/10.1021/acssynbio.4c00070 (2024).
33. Farmani, A. & Moradiani, F. Fabrication friendly NIR-II plasmonics hybrid graphene metasurfaces biosensor: A 3D-FDTD study. *Plasmonics* **20** (11), 10145–10155. https://doi.org/10.1007/s11468-025-03090-5 (2025).
34. Zare, M. S., Attariabad, A., Seyedmasoumian, S. & Farmani, A. High-Quality-Factor, compact nanoplasmonic filter utilizing graphene metasurface at Near-Infrared range. *Adv. Photonics Res.* **6** (8). https://doi.org/10.1002/adpr.202400186 (2025).
35. Omidniaee, A., Karimi, S. & Farmani, A. Surface plasmon Resonance-Based SiO2 Kretschmann configuration biosensor for the detection of blood glucose. *Silicon* **14** (6), 3081–3090. https://doi.org/10.1007/s12633-021-01081-9 (2021).

36. He, Z. et al. Principle and applications of the coupling of surface plasmons and excitons. *Appl. Sci.* **10** (5), 1774. https://doi.org/10.3390/app10051774 (2020).
37. Eghbali, A., Vyshnevyy, A. A., Arsenin, A. V. & Volkov, V. S. Optical anisotropy and excitons in MoS2 interfaces for sensitive surface plasmon resonance biosensors. *Biosensors* **12** (8), 582. https://doi.org/10.3390/bios12080582 (2022).
38. Bruna, M. & Borini, S. Optical constants of graphene layers in the visible range. *Appl. Phys. Lett.* **94** (3), 031901 (2009).
39. Hossain, M. B. & Rana, M. M. Graphene coated high sensitives urface plasmon resonance biosensor for sensing DNA hybridization. *Sens. Lett.* **14**, 1–8 (2016).
40. Hossain, M. B. & Rana, M. M. DNA hybridization detection based on resonance frequency readout IngrapheneonAuSPRbiosensor. *J. Sens.* **16**, 1–8 (2016).
41. Maurya, J. B., Prajapati, Y. K., Singh, V., Saini, J. P. & Tripathi, R. Performance of graphene–MoS2 based surface plasmon resonance sensor using silicon layer. *Opt. Quant. Electron.* **47**, 3599–3611 (2015).
42. Tiwari, J. N., Tiwari, R. N. & Kim, K. S. Zero-dimensional, one-dimensional, two dimensional andthree-dimensional nanostructured materials for advancedelectro chemical energy devices. *Prog Mater. Sci.* **57**, 724–803 (2012).
43. Rahman, M. S., Anower, M. S., Hasan, M. R., Hossain, M. B. & Haque, M. I. Design and numerical analysis of highly sensitive Au-MoS2-graphene based hybrid surface plasmon resonance biosensor. *Opt. Commun.* **396**, 36–43. https://doi.org/10.1016/j.optcom.2017.03.035 (2017).
44. Verma, A., Prakash, A. & Tripathi, R. Sensitivity enhancement of surface plasmon resonance biosensor using graphene and air gap. *Opt. Commun.* **357**, 106–112 (2015).
45. Mousania, Y., Karimi, S. & Farmani, A. Designing High-Performance SPR biosensor using hybrid structure of BifeO3 and 2D material for SARS-CoV-2 detection. *Plasmonics* **20** (9), 7209–7228. https://doi.org/10.1007/s11468-024-02516-w (2025).
46. Mansuri, M., Mir, A. & Farmani, A. Numerical analysis of tunable nonlinear plasmonic router based on nanoscale ring resonators. *Opt. Quant. Electron.* **52** (10). https://doi.org/10.1007/s11082-020-02568-2 (2020).
47. Biednov, M., Lebyedyeva, T. & Shpylovyy, P. Gold and aluminum based surface plasmon resonance biosensors: sensitivity enhancement. *Proc. Opt. Ensors*. **9506**, 95061P (2015).
48. Xia, L., Yin, S., Gao, H., Deng, Q. & Du, C. Sensitivity enhancement for surface plasmon resonance imaging biosensor by utilizing gold–silver bimetallic film configuration. *Plasmonics* **6**, 245–250 (2011).
49. Maurya, J. B., Prajapati, Y. K., Singh, V., Saini, J. P. & Tripathi, R. Improved performance of the surface plasmon resonance biosensor based on graphene or MoS2 using silicon // Opt. Commun. V. 359. P. 426–434. Elsevier BV.

Author contributions

E.B. Design, Analysis, Investigation, Writing-original draft, ConceptualizationH.K. Investigation, Writing-review & editing, Supervision, Project administration, ConceptualizationS.G.S. Investigation, Writing-review & editing, Advising, Validation, Conceptualization.

Funding

"This research did not receive any specific funding."

Declarations

Competing interests

The authors declare no competing interests.

Additional information

Correspondence and requests for materials should be addressed to H.K.